BNL-108512-2015-JA

Operando characterization of catalysts with a portable microreactor

Shen Zhao[a][b], Yuanyuan Li[c], Eli Stavitski[d], Ryan Tappero[d], Stephen Crowley[e], Marco J. Castaldi[e], Dmitri N. Zakharov,[b] Ralph G. Nuzzo[a], Anatoly I. Frenkel[*,c], and Eric A. Stach[*,b]

Abstract: To provide new understandings of the mechanisms of catalytic reactions, improved methods are needed than can monitor changes in the electronic, structural and chemical properties of catalysts, doing so in the *operando* conditions in which catalysts work. We describe here a microreactor-based approach that integrates the capabilities of advanced x-ray, electron, optical and gas-phase compositional analysis techniques in operando conditions. For several exemplary catalytic systems, we demonstrate how this approach enables characterization of three major factors contributing to structure-property correlations evidenced in heterogeneously catalysed reactions, namely: the atomic structure and elemental compositions of nanocatalysts; the physicochemical properties of the support and catalyst-support interfaces; and the gas and surface-phase chemistry occurring under operando conditions. We highlight the generality of the approach as well as outline opportunities for future developments.

Introduction

Recent years have seen an accelerating pace of progress in research focused on the mechanisms of action that mediate heterogeneously catalyzed chemical reactions, investigations that have come to develop a much more vibrant picture of the dynamic structural complexities that are found in such systems. It is now understood, for example, that structure is a feature of heterogeneous catalysts subject to change during chemical transformations occurring at the high tempertature and pressure conditions at which most catalytic processes operate. The fundamental features of such forms of dynamic, operation-specific, transformations are only now beginning to be understood, a feature underpinning an important opportunity for progress in research addressing to methods of characterization applicable to the study of heterogeneous catalysts.[1] Restructuring commonly refers to the changes that occur in bonding structure and composition, and operando-mediated transformations of this form might result in changes in the bonding environments of either near surface atoms (most common), the catalyst cluster shape, and perhaps most importantly the compositional motif (e.g., random alloy to core-shell) of individual metal nanoparticles (NPs).[2] It is a particularly important point to note that most heterogeneous catalysts, and even the well-defined model systems used to study them, are not single-phase/elementary composition solids, but rather present as a system comprised of distributions of size and composition that can be quite important to the chemistry they support. In this context, then, *operando* forms of restructuring can either lead to or be accompanied by changes in the overall properties of these ensembles, e.g., size, shape and degrees of crystalline order.[3] These changes are caused either by: (a) interactions between the metal and the support; and/or (b) interactions resulting form the catalytic reaction itself, including the formation, adsorption, desorption and decomposition of reactants, intermediates and products. Different experimental techniques have been developed to probe such aspects of heterogeneous catalytic processes, with much emphasis being given to experimental and theoretical means that address the atomistic underpinnings of mechanisms of action. Even so, the ability to unify various forms of measurement within a common description of a mechanism, remains limited. Taking as an example studies made of supported transition metal nanoscale catalysts, transmission electron microscopy (TEM) is able to elucidate features related to the morphology, crystal structure and (to some degree) the nature of the electronic structure of individual nanoparticles, as well as to provide a statistical overview of the relative distribution of NP size.[4] X-ray absorption spectroscopy (XAS) describes both the electronic state of the nanoparticles (through the use of the X-ray absorption near edge structure - XANES) and the size, shape and atomic arrangements of an 'average particle' (through analysis of the extended x-ray absorption fine structure spectroscopy - EXAFS).[5] Electron energy loss spectroscopy (EELS)[6] probes electronic structure and composition of both the metal nanoparticle and the support, and thus can be used to probe metal-support interactions in distinguishing, and atomistically-rationalized, ways. Raman spectroscopy[7] can provide information about chemical state and molecular vibrations occurring in oxide supports, and thus can probe transformations in structure of the support that can occur in reaction conditions. Finally, infrared spectroscopy (IR), gas chromatography (GC) and residual gas analysis (RGA) can all be used to describe gas phase and surface species of reactants, intermediates and products during catalytic reactions.[8]

The requirements for progress, however, are ones that can only be addressed through the development of more accurate

[a] Department of Chemistry, University of Illinois, Urbana, IL 61801
[b] Center for Functional Nanomaterials, Brookhaven National Laboratory, Upton, NY 11793
[c] Department of Physics, Yeshiva University, New York, NY 10016
[d] Photon Sciences Division, Brookhaven National Laboratory, Upton, NY 11973
[e] Department of Chemical Engineering, City College of New York, New York, NY 10031
*E-mail: anatoly.frenkel@yu.edu ; estach@bnl.gov

atomistic descriptions that surmount the limitations of "ensemble-averaging" structural methods and the requirements for measurement environments that weakly, if at all, replicate those found in a real process environment. Taking EXAFS as an example, the picture of an 'average particle' that emerges from coordination number modeling,[5,9] may not represent an ensemble if the distribution of particle sizes and/or compositions is broad,[9f, 10] and/or if strongly asymmetric bonds - typical for strained nanoparticle surfaces due to intrinsic relaxations or bonding interactions with adsorbates - are present.[11] Recent EXAFS experiments with nanoscaled metal catalysts (both mono and bimetallic) have demonstrated the limitations of this approach to properly document the nature of the structural and compositional habits embedded in even the relatively simple ensembles found within model systems.[10c, 11a] When the distribution of composition or size/shapes is broad, experimental artifacts can cause underestimation of average particle size,[11c] or compositional motifs (e.g. random alloy NPs can be mistaken by as core-shell NPs).[10b] In addition, and most importantly, catalytic materials are subject to reaction driven forms of transformation, where sizes and compositions of catalytic NPs can change dynamically under reaction conditions.[12] These properties of catalysts highlight the need to include a method such as STEM/TEM, which can provide useful statistical analyses of particle size, shape and composition as a means for describing the ensemble attributes of structure present in a catalytic material, as well as their structural and compositional transformation as might occur during chemical reactions.[13]

The capabilities such methods engender notwithstanding, there remains a more fundamental impediment in the advancement of methods of characterization, namely the static nature of many the experimental methods offering capabilities for probing structure at atomic resolution. The techniques described above are often performed *ex-situ* and/or *ex-post-facto*, and thus provide information about the initial and/or final stages of the reaction, hence likely miss features crucial to understanding changes that may be occurring dynamically during the catalytic cycle. The characteristics of operation at elevated temperatures and pressures, as typical for many heterogeneously catalyzed reactions used in the synthesis of fuels and chemicals, as well as specific changes to the process stream feeds can provide strong thermodynamic driving forces that change the structure and composition of both the metal nanoparticle catalysts and their supports, as well as drive reactions along distinct chemical pathways.[3b,14] Perhaps even more importantly, intermediate states of the catalysts, ones overlooked by static measurements, may be the catalytically active ones or at least add to the understanding of the reaction sequence. For these reasons, and in order to understand reaction mechanisms in contexts explicitly relevant to operational conditions, it is imperative to follow transformation kinetics both in real time and in operando. These points frame goals that stand as grand challenges whose address is necessary to foster progress in this important field of research—the factors driving the increasing emphases being given to so called *in-situ* and *operando* techniques in studies of supported catalysts.[15] For the case of *in-situ* characterization, exposures of the sample to more relevant physical conditions (such as at elevated temperatures or high operating pressures) are made in an effort to better mimic real process states. These *in-situ* techniques, while helping to elucidate some features of important structure-property correlations, miss an important element, namely that of function. To understand structure is important but it remains less than useful if not coupled in a clear way to how the molecular constituents are being transformed by the reactions occurring within the system. Without detecting the products of a catalytic reaction process, the relevance of the structural characterization, even if done in situ, to a mechanistic understanding of reaction kinetics is unquestionably lost. During an *operando* characterization, the relevant characterization approach is applied with the catalysts being held "in a working condition", as validated by measurements of the activity, selectivity and/or stability of the catalyst. *Operando* characterization is perhaps the most ideal form of functional materials characterization, not only because it ensures that the measured parameters properly describe the system as it functions, but also because it allows direct links to be made between different experiments done in equivalent conditions.[16]

The importance of *operando* characterization is now broadly accepted, and there have been significant developments in modes of experiment made in this regard. As examples, techniques such as XAS,[17] X-ray diffraction spectroscopy (XRD),[18] Raman spectroscopy,[19] UV-visible spectroscopy (UV-Vis),[20] and IR spectroscopy[21] have all been utilized within *operando* modes of characterization to study working catalytic systems. These techniques benefit from the low scattering cross sections of photons with matter, which allow deep penetration into materials, greatly simplifying the types of reactor designs which can be utilized for *operando* characterization. Techniques such as transmission electron microscopy (TEM), X-ray photoelectron spectroscopy (XPS), and scanning tunneling microscopy (STM) are more challenging to perform under ambient or even harsh reaction conditions due to the extremely limited travel distance of electrons through moderate pressure or even low-vacuum atmospheres. These techniques normally require high vacuum or ultra-high vacuum (UHV) to function effectively. While differential pumping can provide locally increased pressure environments to the sample, this approach cannot close what is commonly called the "pressure gap" entirely. It has not been possible, even until very recently, to bridge this gap and fully reproduce reactions within an integrated protocol exploiting all of these important modes of experimental characterization.

As the natures of heterogeneously catalyzed reactions can difer very dramatically, there are different types of *operando* studies that have been developed for use within specific fields of research such as electrochemistry,[22] catalysis,[23] and surface science.[24] It has been generally accepted that multiple probes are required to characterize complementary attributes of

catalytic systems, but implementations of this understanding within experiment have varied between different groups.[23,25] Levin and Billinge recently proposed an approach in which available data and theoretical modeling results are optimized for solving a general nanostructure problem.[26] For use within structural and mechanistic studies in catalysis, a limitation exists in the data taken from different instruments often must be measured under a variety of physicochemical states (e.g. some *ex-situ*, some *in-situ* and some *in operando* conditions). Correlating such measurements is challenging because they may probe completely different states of, and possibly completely different forms of, materials systems. An alternative approach of interest in our work is one that makes it possible to perform all *operando* methods characterization across multiple instrumental platforms while maintaining and/or manipulating the sample under identical physicochemical states. While addressing the limitation of the former approach, the latter suffers from a different problem: techniques such as TEM, XPS and STEM cannot be combined with X-ray and other probes, thereby limiting the scope of the problems might be solved in this way.[23]

Recent development of micromachined, enclosed cell reactors (microcells) has enabled *operando* TEM studies of catalytic reactions in ambient atmosphere. With reaction volumes reduced to approximately 10^{-5} mm^3, leading to much lower transport resistance and rates of conversion, and much faster heat and mass transfer rates as a result, the microcells offer distinct advantages in catalytic reaction studies compared to bulk reactors.[27] TEM investigations, now possible at atmospheric pressure due to the closed cell approach and thin window materials, can provide missing information about size, shape and composition of the nanomaterials under *operando* conditions,[28] and, hence, can be used as a unique platform for combining *operando* characterization of the same catalytic process analyzed at different instruments in identical reaction conditions. To illustrate this approach in our previous work, we described the use of a microreactor for correlated studies of Pt catalysts during ethylene hydrogenation reaction by combined XAFS and TEM.[12]

Here we show – through representative examples - how to use this microcell-enabled method of characterization to illuminate the two basic structure-property correlations involving heterogeneous catalysts described above. The essence of our method is illustrated in Figure 1: the same reaction is studied at each facility (synchrotron, electron microscope, etc.) in the same microreactor, while simultaneously probing reactivity using an online residual gas analyzer. To this end, X-ray and infrared microspectroscopy experiments were conducted at the National Synchrotron Light Source (NSLS), STEM/EELS – at the Center for Functional Nanomaterials (CFN), all at Brookhaven National Laboratory. GC/Mass Spectroscopy measurements were conducted at City College of New York (CCNY). The formation of reaction products was detected at each facility, and was used to correlate the data from each instrument, as measured at the same stages of the reaction. Ethylene hydrogenation (and as we show, the concomitant formation of oligomers that are retained by and over tme modify the properties of the support), and carbon monoxide oxidation were chosen as exemplary catalytic reactions and processes for proof of principle demonstrations of the integrated micro-reactor capabilities of interest in this work. STEM, EELS, and XAS characterization were used to obtain structural and electronic information pertaining to the catalyst and support. IR microspectroscopy and Raman spectroscopy were used to identify surface products of the catalysis, and support properties, respectively. Gas chromatography mass spectrometry (GC-MS) and post reactor MS gas analysis (MS) was used for detailed gas phase analysis. Figure 1 shows schematically how the different experimental approaches described above probe different portions of the catalytic system, highlighting the versatility of this newly developed approach.

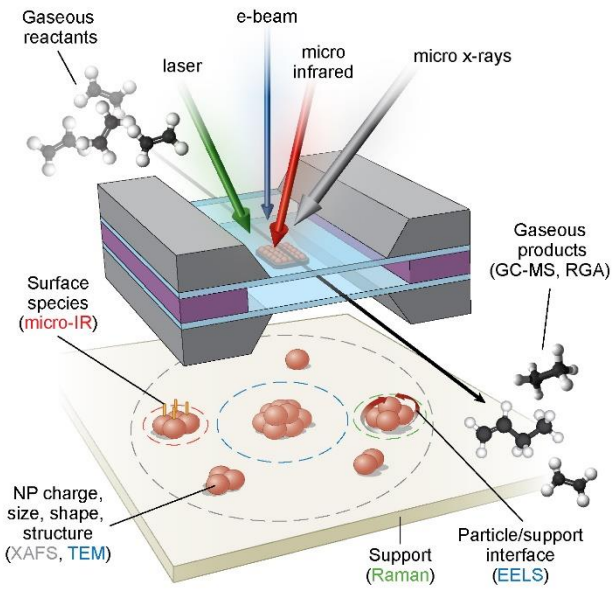

Figure 1. Schematic of the microcell. The catalyst is confined between two silicon nitride windows, and the reaction gases flow through the system, interacting with the confined catalyst at atmospheric pressure. We show how the four different beams (electron, x-ray, infrared, and laser) probe different parts of the catalytic system.

In the discussion that follows in this Article, we present an overview of the design of the microreactor used to integrate this specific multiplatform method of measurement and the data it affords using these individual tests. In the sections that follow, we discuss extensions that can be envisioned that would serve to further its use within measurements exploiting both advanced and developing capabilities of synchrotron sources.

Results and discussion

In this section we present results of exemplary experiments done in the microreactor, grouped according to a particular aspect of a catalytic system they illuminate, namely: 1) the structure and electronic properties of metal catalysts; 2) the nature of support; and 3) the catalytic chemistry. It is important to note that due to the extremely small window area of the microcell (50 by 50 µm), we need to take advantage of micro-focused X-ray and IR beams for all XANES, EXAFS, and IR experiments.

1. Metal catalysts

In this section we present results obtained for the chemical state, structure and statistical distribution of particle sizes of supported Pt and Au catalysts by STEM, XANES and EXAFS.

1.1 Scanning Transmission Electron Microscopy (STEM)

STEM analysis can provide accurate size information to study the morphology and size distribution of the metal NPs. Direct visualization of the size, shape, and dispersion of the metal NPs prior to the reaction is commonly used to describe the initial morphology of the system following catalyst preparation, while ex post facto measurements are commonly used to observe the cumulative changes that occur as a result of the reaction. Additionally, by obtaining the data in *operando* condition, these EM images are able to give statistical information of how these NPs transform (sintering, ripening, and fragmentation) dynamically for the actual catalytic cycle. Compared with techniques such as XAS which often provide averaging particle information, STEM analysis gives local particle information, information that can be critical due to the frequent heterogeneity in NP systems.

Figure 2 shows STEM analysis of particle size distribution and changes in mean particle sizes of Pt-SiO_2 during flow of hydrogen and ethylene at different volumetric ratios.[12] The STEM images shown in Figure 2 were taken at 1 atm pressure. Different stages of the reaction identified in this experiment yield detailed information concerning the size and shape of Pt that change in reaction conditions.[12] For example, after reaching the second hydrogen flow step, following the first ethylene hydrogenation step, a significant number of dumbbell shaped particles were observed, strongly suggesting that motion of the particles on the substrate occurred, indicating the initial stages of sintering (Figure 2c). Interestingly, upon returning the sample to an ethylene rich condition (Figure 2d), these larger agglomerate particles were seen to fracture and form smaller clusters again. A detailed discussion of the origins of these and related phenomena can be found in our prior work.[12] For the purpose of this report, we would like to emphasize the following points: it is possible to obtain high-quality, statistically significant sample of particle size and shape throughout the reaction sequence, all atmospheric pressures of reactive streams. The fact that these observations can be made in significantly rich hydrocarbon streams is both surprising and important. Hydrocarbons often lead to significant contamination during electron microscopy imaging, yet we found that with appropriate considerations of dose and dose rate, it was possible to obtain images with <1nm resolution, even at atmospheric pressures. Observations such as these clearly demonstrate the utility of the microcell approach for operando STEM imaging.

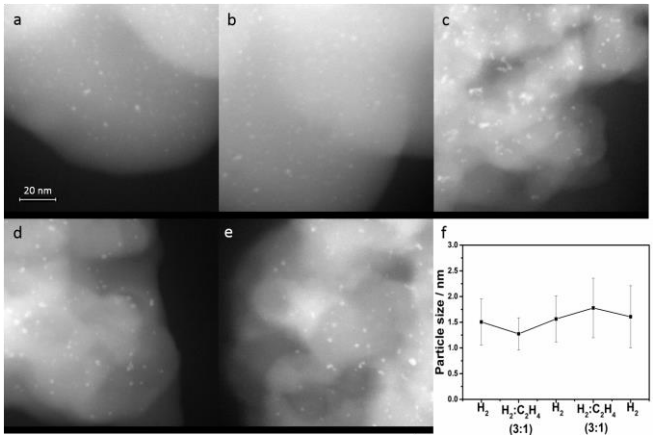

Figure 2. STEM images showing Pt-SiO_2 NPs during different reaction regimes a) pure H_2; b) H_2:C_2H_4=3:1; c) pure H_2; d) H_2:C_2H_4=1:3; e) pure H_2 under 1 atm pressure; f) mean particle size under all 5 reaction regime (only particles not touching each other were counted). All images were taken at room temperature, after the gas flow through the reactor stabilized (ca. 2 hours).[12] The electron dose rate was 600 $e^-/Å^2 \cdot s$.

1.2 X-ray Absorption Near Edge Structure (XANES)

XANES can provide information regarding the electronic structure of metal catalysts. By analyzing the features caused by electronic transitions to empty bound states, XANES is often used to determine both the chemical state and the bonding characteristics of the metal. Figure 3 shows comparison of Au L_3-edge XANES data taken in titania supported Au NPs and bulk Au foil. The NP data were collected in the microreactor using ambient conditions. The Au NPs have an average size of 4 nm, and show metallic XANES features, very similar to bulk Au.

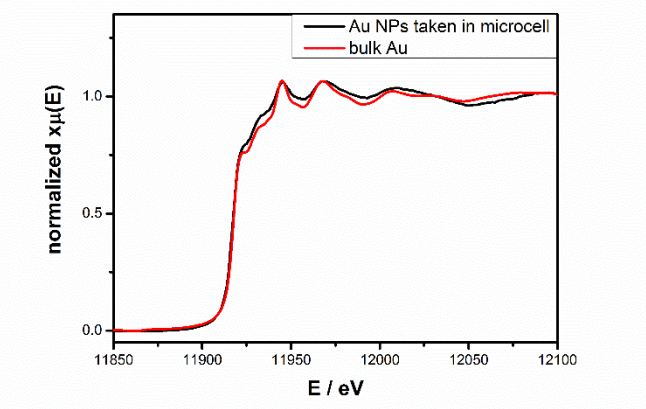

Figure 3. XANES spectra at Au L_3 edge between microcell data for TiO_2 supported Au NPs and bulk Au foil

1.3 Extended X-ray Absorption Fine Structure (EXAFS)

EXAFS is a local structure probe that is based on analysis of the oscillations of the x-ray absorption coefficient that extend to approximately 1000-1500 eV above the absorption edge of an X-ray absorbing atom. The technique can provide structural information such as the distance between the neighboring atoms, their coordination numbers, and bond length disorder, as well as the changes in these quantities under different reaction regimes. Figure 4 shows Fourier transform magnitudes of EXAFS data collected in Au NPs supported by Al_2O_3. The spectra were collected during the flow of mixture of CO and O_2 (1:10 ratio), and in helium before and after the gas mixture flow. One can see irreversible changes in the intensity of the peaks in the range of 2-3.4 Å that occurred during the gas mixture flow, due to, possibly, changes in the metal-metal coordination numbers and, hence, the irreversible growth of Au nanoparticles.

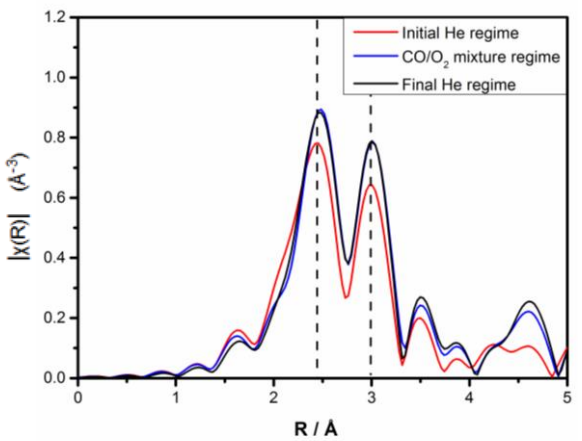

Figure 4. Fourier transform magnitudes of Au L_3 edge k^2-weighted EXAFS spectra measured *in situ* for Au-Al_2O_3 under helium and under the flow of CO and O_2 at 1:10 ratio.

Quantitative data analysis (Table 1) confirmed this hypothesis. Data were analyzed by conventional procedures using IFEFFIT data analysis package and FEFF6 code.[29] Coordination numbers, correction to Au-Au distances and their disorders were varied in the fits, together with the correction to the photoelectron energy origin. The latter parameters were constrained to be the same for all three data sets, to minimize correlation of fitting parameters.

Table 1. Best fit results for Au-Au coordination numbers, bond lengths and their disordered in Au-Al_2O_3 under different atmospheric regimes, obtained by EXAFS analysis of data shown in Figure 4. The last column shows correction to the photoelectron energy origin.

Condition	N_{Au-Au}	R_{Au-Au} (Å)	σ^2(Å^2)	ΔE_0 (eV)
He initial	7.3±0.9	2.846±0.008	0.0062±0.007	6.8±0.6
CO & O_2	8.9±1.1	2.867±0.006	0.0062±0.007	6.8±0.6
He final	8.9±1.0	2.867±0.006	0.0062±0.007	6.8±0.6

In summary of this section, we have shown how both STEM and XAS can be used to quantify the electronic and structural information of metal catalysts during realistic *in situ* and *operando* conditions. The representative data quality is good, thus enabling quantitative analysis of catalysts during reaction conditions by these techniques.

2. Properties of catalytic support

In this section we present results obtained for probing silica and titania supports using EELS and Raman spectroscopy.

2.1 Electron Energy Loss Spectroscopy (EELS)

EELS is an electron analogue to XAS, whereby a magnetic spectrometer is used to separate the electrons that have left the sample according to the energy that they have lost during inelastic interactions with atoms in the sample. Thus, it offers insights into electronic structure of the target supporting materials in a manner that is analogous to XANES. In addition, it is possible to perform nanometer scale chemical mapping using EELS (in either the STEM-EELS spectrum imaging mode, or through so-called energy-filtered imaging – EFTEM). Thus, EELS can probe the composition and electronic structure of individual NPs, information that can be critical to understanding the fundamental chemistry of catalytic reactions. Additionally, the catalytic properties of a system can depend greatly on the interface between the metal and the support: EELS has the potential to directly observe electronic structure changes that occur in the supporting materials during reaction, and thus can describe such important effects as the interaction between the metal and support. Here we show just one example taken from the Si L edge obtained at atmospheric pressure in the microcell for the Pt-SiO_2 sample. It is important to point out the microcell consists of two SiN windows, and thus any contribution to the Si L edges necessarily consists of signal from the two membrane windows.

Figure 5 showed changes in the Si EELS spectra collected during the flow of 3:1 H_2:C_2H_4 mixture over Pt/SiO_2 catalysts in the ethylene hydrogenation experiment described in the previous section. In addition to the spectrum obtained with the sample loaded in the cell, a spectrum obtained in control experiment without the sample is shown as well, to subtract the effect due to the SiN windows. The two strong peaks at 108 and 115 eV are associated with Si-O bonds[30] that exhibit transformation in response to reaction conditions.

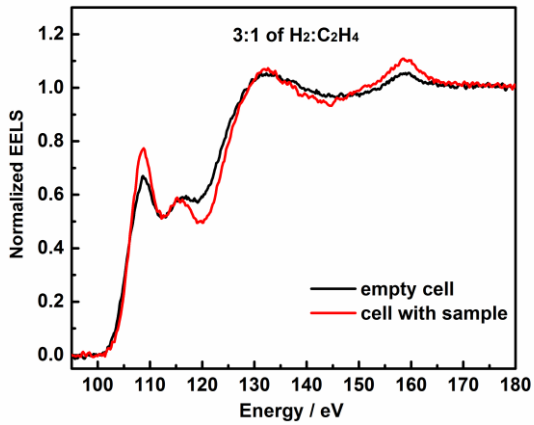

Figure 5. *Operando* EELS spectra of Si L-edge under different reaction regimes (from insert). The individual spectra show difference in near edge structure that depend on the nature of the reactive environment.

2.2 Raman spectroscopy

Raman spectroscopy provides fingerprints of molecules and/or crystal structures by probing their vibrational properties. Most recently, *operando* Raman spectroscopy was combined with XAS in the same experiments, to correlate changes in catalysts with changes in support materials under reaction conditions.[25a,31] Raman spectra can be used to determine the crystalline phase of different commonly used catalytic supports, such as, e.g., TiO_2.[32] Figure 6 shows a comparison made of representative Raman spectra for pure TiO_2 probed in a microreactor and larger (quartz capillary) tube reactor. Positions of Raman bands observed in the both cells are in good agreement with those expected for an anatase structure. The well resolved peak at 145 cm^{-1} is assignable to the main anatase vibrational mode. In addition, modes at 397 (B_{1g}), 517 (A_{1g}) and 638 (E_g) cm^{-1} are seen in both spectra, indicating the majority of the sample was present in the crystalline form.[33]

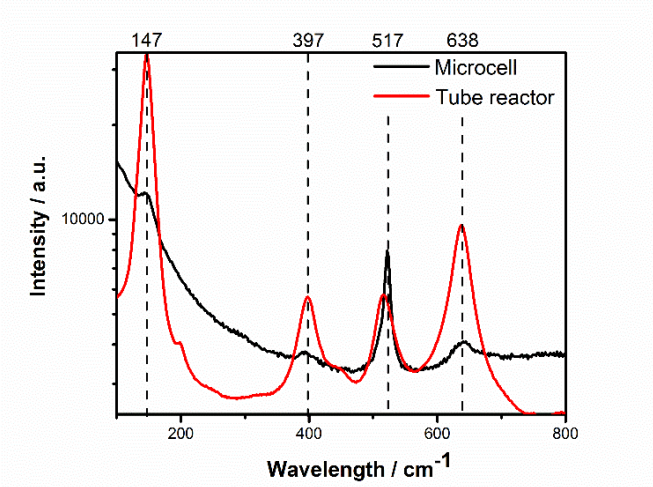

Figure 6. Raman spectra of pure TiO_2 (anatase) taken in microcell and conventional tube reactor

The fact that both spectra show very similar features demonstrates the feasibility of employing the microcell for Raman measurements made both *in situ* and under *in operando* conditions.

3. Catalytic chemistry

In this section we present exemplary data on detection of gas phase and surface species formed during catalytic reactions.

3.1 Surface catalytic intermediates and products analysis

IR spectroscopy is a powerful technique to perform surface analysis of adsorbates that can bind to both metals and supports. *Operando* IR spectroscopy can thus contribute vitally important data for understanding the surface chemistry of a catalyst in real time. Figure 7 presents time resolved synchrotron IR microspectroscopy data obtained for the same conditions of the ethylene hydrogenation reaction experiment as described in section 1. The data in Figure 7 are ones measured for the stoichiometric reaction condition (H_2:C_2H_4=1:1) as a function of time. These results show directly the formation and retention on the support of aliphatic hydrocarbon products formed during the ethylene hydrogenation process via a competing, and generally low yield, competing oligomerization pathway. IThe aliphatic speciation implied here is supported by the fact that the modes appearing in the C-H stretching region (the three peaks centered at 2958, 2918 and 2850 cm^{-1}) under operando reaction conditions are ones directly assignable the group C-H stretching frequencies of (linear) hydrocarbons. The significant growth at peak 2918 cm^{-1} (asym. CH_2 stretch) and 2850 cm^{-1} (sym. CH_2 stretch) indicating heavier oligomers are formed and accumulate on/within the support over time.

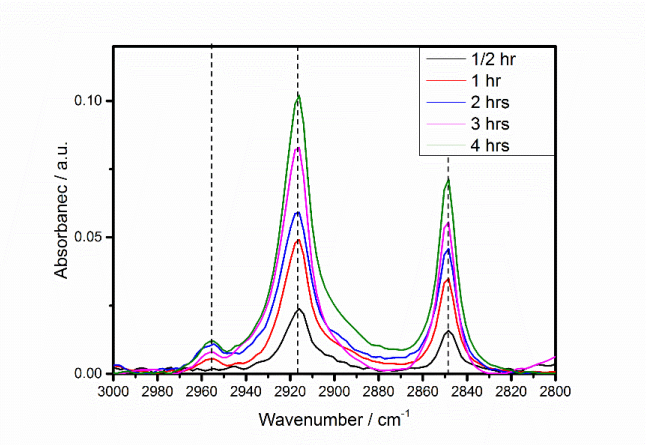

Figure 7: Time resolved IR spectra collected during room temperature ethylene hydrogenation over Pt-SiO_2 catalysts.

By examining the IR spectra taken in microcell, we were able to detect subtle changes of the surface species that were formed on the Pt catalyst and/or support. The experiment illustrates potential of this method for measuring surface species (reactants, intermediates and products) using the microcell.

3.2 Gas phase catalytic products analysis

RGA and GC-MS can be used to identify and quantify gas phase products and thus help in studies of catalytic reaction kinetics. Examples of their use are shown in Figures 8 and 9. Figure 8 is the gas chromatogram for ethane and ethylene elution during ethylene hydrogenation reaction over Pt-SiO_2 catalyst, described previously, at stoichiometric reaction condition (H_2:C_2H_4=1:1). The ethane and ethylene peaks were well separated. Irregular shape of the ethylene peak was due to the large amount of ethylene in the GC sample loop yet still quantifyable. Due to the extremely small loading of the catalyst in the microcell, ethane production was small but still yielded a significant signal to noise ratio, suggesting that GC-MS can be utilized to measure gas phase product formation directly from the microcell output.

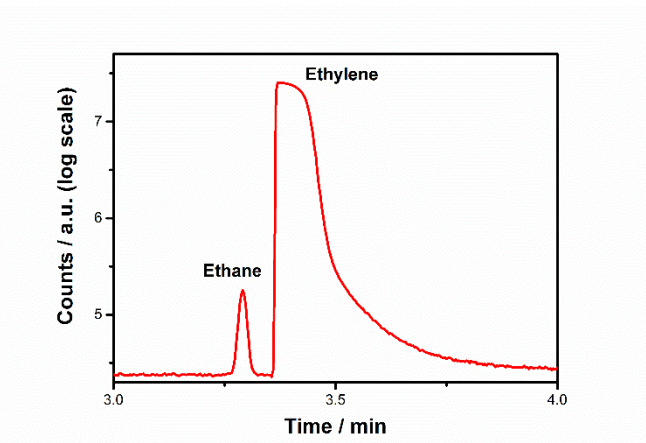

Figure 8. Gas chromatogram showing reactant (ethylene) and product (ethane) for ethylene hydrogenation over Pt-SiO_2

RGA data was taken from the output of the microcell, in the same condition as the GC-MS experiment described above and shown in Figure 8. Figure 9 shows that ethane production increases under ideal, stoichiometric reaction conditions (1:1 ratio of hydrogen to ethylene) compared to the baseline experiment where pure ethylene was fed to the cell.

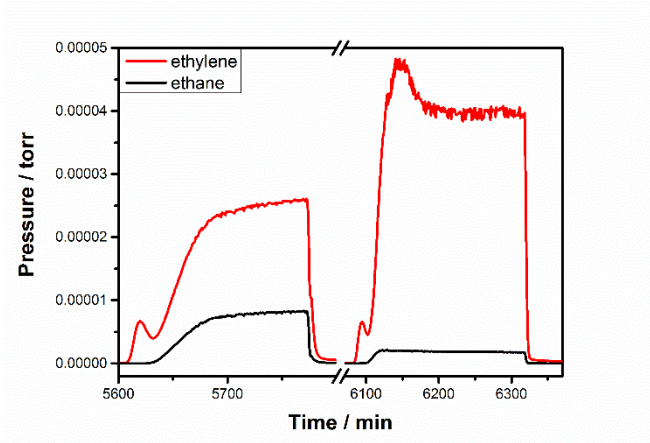

Figure 9. RGA data comparison showing the pressure of reactant (ethylene) and product (ethane) between H_2:C_2H_4=1:1 reaction condition and pure ethylene condition.

Both GC-MS and RGA results show the unambiguous evidence that catalytic ethylene conversion in the microcell can be dedected by analyzing gas phase composition downstream of the cell. Both techniques provide valuable insights on revealing catalytic mechanism and kinetic of ethylene hydrogenation reaction over Pt-SiO_2 catalyst.

The above data collected in several proof-of-principle experiments demonstrate the ability of different techniques to probe catalytic system in the microreactor. In most cases, these data were complemented by corresponding reaction data collected online in parallel with catalyst characterization. Our method, therefore, shows strong promise for combined, *operando* studies of catalytic reactions that circumvent the main limitations of the existing approaches (*ex-situ* combinations of all relevant methods[26], and *in-situ/operando* combinations of multiple techniques in the same experiment[23a]) Due to low heat and mass transfer, and low conversion rates, microreactor studies of reaction kinetics have unique advantage over bulk reactors used in *operando* characterization.

With further development and application of the microreactor and new methods of integrating it with multiple experimental facilities, it is envisioned that this approach will see even broader utilization. While all of the results shown above have been obtained from catalyzed chemical reactions that occur during room temperature, recent developments in microcell fabrication have led to the creation of systems that can achieve quite high temperatures.[34] They have shown nanoscale TEM and STEM imaging at temperatures as high as 800 °C, with temperatures of 500 °C being able to be maintained in highly aggressive environments for many hours before heating element failure.

Additionally, there do not appear to be strong restrictions to the use of microfabricated reactors in a variety of additional experimental approaches relevant to the characterization of nanoparticle catalysts. These include bulk probes such as x-ray diffraction and x-ray and electron pair distribution function analysis, as well as focused, nanoprobe x-ray probes such as nanodiffraction, transmission x-ray and scanning transmission x-ray imaging. Importantly, quantitative stable gas phase measurements can be obtained via RGA and GC-MS to fully understand the catalytic cycle. Furthermore, with increasing development of the approach it is possible that x-ray photoelectron spectroscopy may also be included in the characterization suite.[35]

Conclusions

The discussions above illustrate the scope and diversity of the forms of data that can be measured in integrated form using a common reactor microcell. Different types of microscopy (STEM) and spectroscopy (EELS, XAS, IR, and Raman) were utilized to provide new insights into the nature of the structure-property relationships that exist in prototypical catalytic reactions under in *operando* conditions. In this work, we selected ethylene hydrogenation and CO oxidation as exemplary reactions, using them to demonstrate the unique qualities and inherent practicality of the multiplatform integration made possible through the use of and integrated microcell methodology. This approach features a cell design specifically enabling the features needed for combined studies of type, and in ways that can be exploited for investigations of essentially any catalytic reaction under experimental conditions approaching those of operando states. The highlights presented above, when taken together with our recently reported work on the mechanisms that operate in the dynamic transformation of supported platinum nanocluster catalysts during the ethylene hydrogenation reaction illustrates an approach could in principle be applied as a general methodology within the broader field of *operando* research in heterogeneous catalysis.

Experimental Section

Cell Design

The microcell consists of two 50 by 50 µm SiN windows with 500 nm spacing in between connected to three capillary channels (inlet, outlet, and bypass). The catalyst is loaded between the two windows and reactants are introduced into the cell using mass flow controllers (MFCs) and pressure controllers was equipped to provide desired pressure and steady flow rate.

Experiments with Micro-reactor:

Experiments with the micro-reactor are summarized below. They are grouped according to the experimental facility used. When appropriate, they are characterized as either *ex-situ*, *in-situ*, or *operando* experiments.

In studying real time reactivity, mixtures of various feed gases (hydrogen and ethylene or carbon monoxide and oxygen) of variable compositions were flown through the reactor cell. The pressure in the flow microcell was slightly above atmospheric pressure (1000 torr).

Electron microscopy experiments were performed using a Titan 80-300 Environmental Transmission Electron Microscope at the Center for Functional Nanomaterials, Brookhaven National Laboratory. Annular dark field scanning transmission electron microscopy images were acquired at a constant image magnification of 640,000 times magnification operating at 300 keV.

The XANES and EXAFS measurements were performed at beamline X27A, National Synchrotron Light Source (NSLS). The microcell was mounted on the stage approximately 45 degrees to the incident X-ray beam and the emitted fluorescence was detected from the downstream side of the cell by 4 channel Vortex detector. All XAFS spectra were recorded after the gases reached stable state.

The IR microspectroscopy experiments were performed using the N_2 purged Thermo Nicolet Magna 860 Step-Scan FT-IR and Spectra Tech Continuµm IR Microscope at the U2B beamline (NSLS). The IR measurements were performed under continuous gas flow with 4 cm^{-1} spatial resolution and 256 scans.

Raman spectra for all TiO_2 films were collected using a Bay Spec spectrometer equipped with a 532 nm laser excitation. The spectrometer was calibrated using a silicon wafer to a wave number accuracy of ±1 cm^{-1}. A non-contact fiber optic HT probe objective was used for beam focusing and collection of scattered radiation. 5 spectra were accumulated with a 30 s exposure time. The resulting total spectral recording time was 150 s. The laser output power was 23 mW.

An on-line GC-MS system (Agilent 7890A GC equipped with 5975c MS detector) equipped with a GS-GasPro column (Agilent 60m by 0.32mm) was used to analyze gas phase compounds. Helium (UHP grade) was used as carrier gas in constant flow mode. The oven temperature was programmed from 40°C to 150°C at ramping rate of 20°C/min, held at 150°C for 1min, then ramped to 200°C at rate of 20°C/min and held for 3min. The temperature of quad and source of MSD were set to be 180°C and 230°C, respectively.

An RGA (SRS) was used to monitor the real-time mass production for CO oxidation reactions. It was connected to the outlet of the microcell for the experiments described above.

Acknowledgements

We thank A. Patlolla for help with Raman spectroscopy measurements, R. Anderson for making sampels for CO oxidation experiment, U. Jung and A. Elsen for making samples for ethylene hydrogenation. The authors gratefully acknowledge funding of this work by the Division of Chemical Sciences, Geosciences, and Biosciences within the U. S. Department of Energy Office of Basic Energy Sciences, Grant No. DE-FG02-03ER15476 (S.Z., Y.L., R.G.N., A.I.F., and E. A.S.). The development of the micro-cell was supported, in part, by an LDRD grant at Brookhaven National Laboratory (E. A. S., and A. I. F.). We acknowledge the facilities support provided at the Centre for Functional Nanomaterials, the National Synchrotron Light Source at the Brookhaven National Laboratory (US Department of Energy, Office of Basic Energy Sciences,

Contract No. DE-SC0012704) and the Synchrotron Catalysis Consortium (US Department of Energy, Office of Basic Energy Sciences, Grant No. DE-SC0012335).

Keywords: heterogeneous catalysis • microcell • *operando* characterization

References:

[1] a) Y. G. Sun, Y. N. Xia, *Science* **2002**, *298*, 2176-2179; b) S. Polarz, A. Roy, M. Lehmann, M. Driess, F. E. Kruis, A. Hoffmann, P. Zimmer, *Adv. Funct. Mater.* **2007**, *17*, 1385-1391; c) K. Kohler, R. G. Heidenreich, S. S. Soomro, S. S. Prockl, *Adv. Synth. Catal.* **2008**, *350*, 2930-2936; d) J. Kugai, T. Moriya, S. Seino, T. Nakagawa, Y. Ohkubo, H. Nitani, T. A. Yamamoto, *Int. J Hydrogen. Energ.* **2013**, *38*, 4456-4465.

[2] a) G. A. Somorjai, Y. Borodko, *Catal. Lett.* **1999**, *59*, 89-91; b) F. Tao, S. R. Zhang, L. Nguyen, X. Q. Zhang, *Chem. Soc. Rev.* **2012**, *41*, 7980-7993; c) F. Tao, M. E. Grass, Y. W. Zhang, D. R. Butcher, J. R. Renzas, Z. Liu, J. Y. Chung, B. S. Mun, M. Salmeron, G. A. Somorjai, *Science* **2008**, *322*, 932-934; d) S. Wunder, Y. Lu, M. Albrecht, M. Ballauff, *ACS Catal.* **2011**, *1*, 908-916.

[3] a) L. Li, L. L. Wang, D. D. Johnson, Z. F. Zhang, S. I. Sanchez, J. H. Kang, R. G. Nuzzo, Q. Wang, A. I. Frenkel, J. Li, J. Ciston, E. A. Stach, J. C. Yang, *J Am Chem Soc* **2013**, *135*, 13062-13072; b) T. W. Hansen, J. B. Wagner, Acs Catal 2014, 4, 1673-1685; c) D. S. Su, B. S. Zhang, R. Schlogl, Chem Rev 2015, 115, 2818-2882; d) S. B. Vendelbo, C. F. Elkjaer, H. Falsig, I. Puspitasari, P. Dona, L. Mele, B. Morana, B. J. Nelissen, R. van Rijn, J. F. Creemer, P. J. Kooyman, S. Helveg, Nat Mater 2014, 13, 884-890.

[4] a) Z. L. Wang, *Adv. Mater.* **2003**, *15*, 1497-1514; b) J. C. Yang, M. W. Small, R. V. Grieshaber, R. G. Nuzzo, *Chem. Soc. Rev.* **2012**, *41*, 8179-8194.

[5] a) A. I. Frenkel, *J. Synchrotron Radiat.* **1999**, *6*, 293-295; b) A. I. Frenkel, C. W. Hills, R. G. Nuzzo, *J. Phys. Chem. B* **2001**, *105*, 12689-12703.

[6] B. K. Miller, P. A. Crozier, *Microsc. Microanal.* **2014**, *20*, 815-824.

[7] I. E. Wachs, C. A. Roberts, *Chem. Soc. Rev.* **2010**, *39*, 5002-5017.

[8] a) A. Corma, L. T. Nemeth, M. Renz, S. Valencia, *Nature* **2001**, *412*, 423-425; b) P. Shen, S. Zhao, D. Su, Y. Li, A. Orlov, Appl. Catal. B-Environ. **2012**, 126, 153-160; c) I. E. Wachs, *Catal. Today* **1996**, *27*, 437-455.

[9] a) M. S. Nashner, A. I. Frenkel, D. L. Adler, J. R. Shapley, R. G. Nuzzo, *J. Am. Chem. Soc.* **1997**, *119*, 7760-7771; b) A. Jentys, *Phys. Chem. Chem. Phys.* **1999**, *1*, 4059-4063; c) S. Calvin, M. M. Miller, R. Goswami, S. F. Cheng, S. P. Mulvaney, L. J. Whitman, V. G. Harris, *J. Appl. Phys.* **2003**, *94*, 778-783; d) B. R. Cuenya, J. R. Croy, S. Mostafa, F. Behafarid, L. Li, Z. F. Zhang, J. C. Yang, Q. Wang, A. I. Frenkel, *J. Am. Chem. Soc.* **2010**, *132*, 8747-8756; e) A. Frenkel, *Z. Kristallogr.* **2007**, *222*, 605-611; f) A. I. Frenkel, *Chem. Soc. Rev.* **2012**, *41*, 8163-8178; g) A. M. Beale, B. M. Weckhuysen, *Phys. Chem. Chem. Phys.* **2010**, *12*, 5562-5574.

[10] a) G. Agostini, R. Pellegrini, G. Leofanti, L. Bertinetti, S. Bertarione, E. Groppo, A. Zecchina, C. Lamberti, *J. Phys. Chem. C* **2009**, *113*, 10485-10492; b) A. I. Frenkel, Q. Wang, S. I. Sanchez, M. W. Small, R. G. Nuzzo, *J. Chem. Phys.* **2013**, *138*; c) A. I. Frenkel, A. Yevick, C. Cooper, R. Vasic, *Annu. Rev. Anal. Chem.* **2011**, *4*, 23-39.

[11] a) S. T. Chill, R. M. Anderson, D. F. Yancey, A. I. Frenkel, R. M. Crooks, G. Henkelman, *ACS Nano* **2015**, *9*, 4036-4042; b) O. M. Roscioni, N. Zonias, S. W. T. Price, A. E. Russell, T. Comaschi, C. K. Skylaris, *Phys. Rev. B* **2011**, *83*; c) A. Yevick, A. I. Frenkel, *Phys. Rev. B* **2010**, *81*.

[12] Y. Li, D. Zakharov, S. Zhao, R. Teppero, U. Jung, A. Elsen, Ph. Baumann, R. G. Nuzzo, E. A. Stach, A. I. Frenkel, *Nat. Comm*. **2015**, *6*,7583-7588.

[13] a) H. L. L. Xin, S. Alayoglu, R. Z. Tao, A. Genc, C. M. Wang, L. Kovarik, E. A. Stach, L. W. Wang, M. Salmeron, G. A. Somorjai, H. M. Zheng, *Nano Lett.* **2014**, *14*, 3203-3207; b) H. L. Xin, E. A. Pach, R. E. Diaz, E. A. Stach, M. Salmeron, H. M. Zheng, *ACS Nano* **2012**, *6*, 4241-4247.

[14] a) D. Gamarra, G. Munuera, A. B. Hungria, M. Fernandez-Garcia, J. C. Conesa, P. A. Midgley, X. Q. Wang, J. C. Hanson, J. A. Rodriguez, A. Martinez-Arias, *J. Phys. Chem. C* **2007**, *111*, 11026-11038; b) A. Hopkinson, D. A. King, *Chem Phys* **1993**, *177*, 433-452; c) T. Mallat, A. Baiker, *Appl. Catal. a-Gen.* **2000**, *200*, 3-22.

[15] a) D. R. Baer, M. H. Engelhard, G. E. Johnson, J. Laskin, J. F. Lai, K. Mueller, P. Munusamy, S. Thevuthasan, H. F. Wang, N. Washton, A. Elder, B. L. Baisch, A. Karakoti, S. V. N. T. Kuchibhatla, D. Moon, *J. Vac. Sci. Technol. A* **2013**, *31*; b) M. A. Banares, *Adv. Mater.* **2011**, *23*, 5293-5301; c) M. A. Banares, I. E. Wachs, *J. Raman Spectrosc.* **2002**, *33*, 359-380; d) A. I. Frenkel, J. A. Rodriguez, J. G. G. Chen, *ACS Catal.* **2012**, *2*, 2269-2280; e) S. Lwin, I. E. Wachs, *ACS Catal.* **2014**, *4*, 2505-2520; f) A. M. Molenbroek, S. Helveg, H. Topsoe, B. S. Clausen, *Top. Catal.* **2009**, *52*, 1303-1311; g) J. A. Rodriguez, J. C. Hanson, D. Stacchiola, S. D. Senanayake, *Phys. Chem. Chem. Phys.* **2013**, *15*, 12004-12025; h) H. Topsoe, *J. Catal.* **2003**, *216*, 155-164; iB. M. Weckhuysen, *Phys. Chem. Chem. Phys.* **2003**, *5*, 4351-4360.

[16] a) M. A. Banares, *Catal. Today* **2005**, *100*, 71-77; b) S. Deabate, G. Gebel, P. Huguet, A. Morin, G. Pourcelly, *Energ. Environ. Sci.* **2012**, *5*, 8824-8847; c) C. Sievers, S. R. Bare, E. Stavitski, *Catal. Today* **2013**, *205*, 1-2.

[17] a) K. Fottinger, J. A. van Bokhoven, M. Nachtegaal, G. Rupprechter, *J Phys. Chem. Lett.* **2011**, *2*, 428-433; b) J. L. Fulton, J. C. Linehan, T. Autrey, M. Balasubramanian, Y. Chen, N. K. Szymczak, *J. Am. Chem. Soc.* **2007**, *129*, 11936-11949.

[18] J. Kulisch, H. Sommer, T. Brezesinski, J. Janek, *Phys. Chem. Chem. Phys.* **2014**, *16*, 18765-18771.

[19] S. J. Tinnemans, M. H. F. Kox, T. A. Nijhuis, T. Visser, B. M. Weckhuysen, *Phys. Chem. Chem. Phys.* **2005**, *7*, 211-216.

[20] a) A. M. Beale, A. M. J. van der Eerden, K. Kervinen, M. A. Newton, B. M. Weckhuysen, *Chem. Commun.* **2005**, 3015-3017; b) M. H. Groothaert, K. Lievens, H. Leeman, B. M. Weckhuysen, R. A. Schoonheydt, *J. Catal.* **2003**, *220*, 500-512.

[21] a) A. Goguet, F. C. Meunier, D. Tibiletti, J. P. Breen, R. Burch, *J. Phys. Chem. B* **2004**, *108*, 20240-20246; b) T. Lesage, C. Verrier, P. Bazin, J. Saussey, M. Daturi, *Phys. Chem. Chem. Phys.* **2003**, *5*, 4435-4440; c) O. Marie, F. Thibault-Starzyk, P. Massiani, *J. Catal.* **2005**, *230*, 28-37; d) G. Ramakrishnan, S. Zhao, W. Q. Han, A. Orlov, *Chem. Eng. J.* **2011**, *170*, 445-450; e) J. Sirita, S. Phanichphant, F. C. Meunier, *Anal. Chem.* **2007**, *79*, 3912-3918; f) S. Zhao, G. Ramakrishnan, D. Su, R. Rieger, A. Koller, A. Orlov, *Appl. Catal. B-Environ.* **2011**, *104*, 239-244.

[22] a) M. E. Holtz, Y. C. Yu, D. Gunceler, J. Gao, R. Sundararaman, K. A. Schwarz, T. A. Arias, H. D. Abruna, D. A. Muller, *Nano Lett.* **2014**, *14*, 1453-1459; b) J. B. Leriche, S. Hamelet, J. Shu, M. Morcrette, C. Masquelier, G. Ouvrard, M. Zerrouki, P. Soudan, S. Belin, E. Elkaim, F. Baudelet, *J. Electrochem. Soc.* **2010**, *157*, A606-A610; c) M. Tada, S. Murata, T. Asakoka, K. Hiroshima, K. Okumura, H. Tanida, T. Uruga, H. Nakanishi, S. Matsumoto, Y. Inada, M. Nomura, Y. Iwasawa, *Angew. Chem. Int. Edit.* **2007**, *46*, 4310-4315.

[23] a) S. J. Tinnemans, J. G. Mesu, K. Kervinen, T. Visser, T. A. Nijhuis, A. M. Beale, D. E. Keller, A. M. J. van der Eerden, B. M. Weckhuysen, *Catal. Today* **2006**, *113*, 3-15; b) W. Q. Xu, R. Si, S. D. Senanayake, J. Llorca, H. Idriss, D. Stacchiola, J. C. Hanson, J. A. Rodriguez, *J. Catal.* **2012**, *291*, 117-126.

[24] a) F. Tao, *Chemcatchem* **2012**, *4*, 583-590; b) M. A. van Spronsen, G. J. C. van Baarle, C. T. Herbschleb, J. W. M. Frenken, I. M. N. Groot, *Catal. Today* **2015**, *244*, 85-95.

[25] a) A. Patlolla, P. Baumann, W. Xu, S. D. Senanayake, J. A. Rodriguez, A. I. Frenkel, *Top. Catal.* **2013**, *56*, 896-904; b) S. Y. Yao, K. Mudiyanselage, W. Q. Xu, A. C. Johnston-Peck, J. C. Hanson, T. P. Wu, D. Stacchiola, J. A. Rodriguez, H. Y. Zhao, K. A. Beyer, K. W. Chapman, P. J. Chupas, A. Martinez-Arias, R. Si, T. B. Bolin, W. J. Liu, S. D. Senanayake, *ACS Catal.* **2014**, *4*, 1650-1661.

[26] S. J. L. Billinge, I. Levin, *Science* **2007**, *316*, 561-565.

[27] a) G. Kolb, V. Hessel, *Chem. Eng. J.* **2004**, *98*, 1-38; b) G. Kolb, V. Hessel, V. Cominos, C. Hofmann, H. Lowe, G. Nikolaidis, R. Zapf, A. Ziogas, E. R. Delsman, M. H. J. M. de Croon, J. C. Schouten, O. de la Iglesia, R. Mallada, J. Santamaria, *Catal. Today* **2007**, *120*, 2-20; c) G. Sankar, E. H. Cao, A. Gavriilidis, *Catal. Today* **2007**, *125*, 24-28.

[28] a) S. Chenna, P. A. Crozier, *ACS Catal.* **2012**, *2*, 2395-2402; b) M. Gu, L. R. Parent, B. L. Mehdi, R. R. Unocic, M. T. McDowell, R. L. Sacci, W. Xu, J. G. Connell, P. H. Xu, P. Abellan, X. L. Chen, Y. H. Zhang, D. E. Perea, J. E. Evans, L. J. Lauhon, J. G. Zhang, J. Liu, N. D. Browning, Y. Cui, I. Arslan, C. M. Wang, *Nano Lett.* **2013**, *13*, 6106-6112; c) B. L. Mehdi, M. Gu, L. R. Parent, W. Xu, E. N. Nasybulin, X. L. Chen, R. R. Unocic, P. H. Xu, D. A. Welch, P. Abellan, J. G. Zhang, J. Liu, C. M. Wang, I. Arslan, J. Evans, N. D. Browning, *Microsc. Microanal.* **2014**, *20*, 484-492.

[29] S. I. Zabinsky, J. J. Rehr, A. Ankudinov, R. C. Albers, M. J. Eller, Phys. Rev. B **1995**, 52, 2995-3009.

[30] J. Park, S. Heo, J. Chung, G. S. Park, *Microsc. Microanal.* **2013**, *19*, 109-113.

[31] A. Patlolla, E. V. Carino, S. N. Ehrlich, E. Stavitski, A. I. Frenkel, *ACS Catal.* **2012**, *2*, 2216-2223.

[32] a) I. M. Arabatzis, T. Stergiopoulos, D. Andreeva, S. Kitova, S. G. Neophytides, P. Falaras, *J. Catal.* **2003**, *220*, 127-135; b) P. Falaras, A. H. Le Goff, M. C. Bernard, A. Xagas, *Sol. Energ. Mat. Sol. C* **2000**, *64*, 167-184.

[33] Y. Yu, J. C. Yu, J. G. Yu, Y. C. Kwok, Y. K. Che, J. C. Zhao, L. Ding, W. K. Ge, P. K. Wong, *Appl. Catal. a-Gen.* **2005**, *289*, 186-196.

[34] H. L. L. Xin, K. Y. Niu, D. H. Alsem, H. M. Zheng, *Microsc. Microanal.* **2013**, *19*, 1558-1568.

[35] A. Kolmakov, D. A. Dikin, L. J. Cote, J. X. Huang, M. K. Abyaneh, M. Amati, L. Gregoratti, S. Gunther, M. Kiskinova, *Nat. Nanotechnol.* **2011**, *6*, 651-657.

Entry for the Table of Contents (Please choose one layout)

Layout 1:

FULL PAPER

Text for Table of Contents

Schematic of the portable microreactor. The catalyst is confined between two silicon nitride “windows” and the reacting gas mixture flowing through the system. The microreactor is compatible with complementary *operando* characterization techniques.

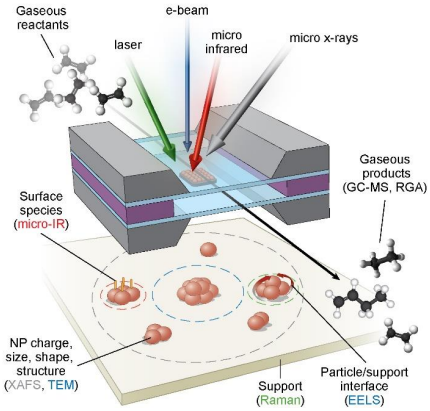

Shen Zhao, Yuanyuan Li, Eli Stavitski, Ryan Tappero, Stephen Crowley, Marco J. Castaldi, Dmitri N. Zakharov, Ralph G. Nuzzo, Anatoly I. Frenkel, and Eric A. Stach**

Page No. – Page No.

Title

Operando characterization of catalysts with a portable microreactor